Final Draft
of the original manuscript:

Hiekkataipale, P.; Loebling, T.I.; Poutanen, M.; Priimagi, A.; Abetz, V.; Ikkala, O.; Groeschel, A.H.:

Controlling the shape of Janus nanostructures through supramolecular modification of ABC terpolymer bulk morphologies

In: Polymer (2016) Elsevier

DOI: 10.1016/j.polymer.2016.05.076

Controlling the shape of Janus nanostructures through supramolecular modification of ABC terpolymer bulk morphologies

Panu Hiekkataipale[1], Tina I. Löbling[1], Mikko Poutanen[1], Arri Priimagi[2], Volker Abetz[3,4] Olli Ikkala[1,*] and Andre. H. Gröschel[1,5,*]

[1] *Department of Applied Physics, Aalto University School of Science, FI-02100 Espoo, Finland.*

[2] *Department of Chemistry and Bioengineering, Tampere University of Technology, FI-33101 Tampere, Finland.*

[3] *Institute of Physical Chemistry, University of Hamburg, D-20146 Hamburg, Germany*

[4] *Institute of Polymer Research, Helmholtz-Zentrum Geesthacht, D-21502 Geesthacht, Germany*

[5] *Physical Chemistry and Centre for Nanointegration (CENIDE), University of Duisburg-Essen, D-45127 Essen, Germany*

Abstract: Block copolymers microphase separate into a variety of bulk morphologies that serve as scaffolds, templates, masks and source for polymeric nano-particles. While supramolecular additives are common to complex within diblock copolymers to modify the morphology, the subtle effects of complexation on ABC triblock terpolymer morphologies are less explored. Here, we describe the manipulation of polystyrene-*block*-poly(4-vinylpyridine)-*block*-poly(*tert*-butyl methacrylate) (PS-*b*-P4VP-*b*-PT or S4VT) triblock terpolymer bulk morphologies through supramolecular complexation with rod-like 4-(4-pentylphenylazo)phenol (5PAP). The 5PAP molecule hydrogen bonds by phenolic groups to the 4VP repeating units and with increasing molar fraction of 5PAP, initially observed P4VP cylinders flatten into elliptic cylinders until a morphological transition occurs into a third (P4VP/5PAP) lamella. At sufficient 5PAP loadings, the cylinders can even merge into a perforated P4VP lamella located at the PS/PT interface. Quaternization of the P4VP phase and re-dispersion in organic solvent allows liberating S4VT Janus nanostructures from the bulk, including Janus cylinders, nanoporous Janus membranes and Janus sheets. The manipulation of "sandwiched" microphases through supramolecular binding motifs could allow the preparation of previously inaccessible terpolymer bulk morphologies and, in case of cross-linkable phases, lead to a larger library of Janus nano-objects.

Keywords: triblock terpolymers; self-assembly; bulk morphologies; Janus nanostructures; perforated lamellae; supramolecular chemistry;

Introduction

The trend towards miniaturization of structures and systems in all fields of science and technology is progressing towards the nano-scale. While top-down approaches for the fabrication of micron-sized features often require sophisticated equipment, bottom-up approaches aim at fabricating the desired material from smaller building blocks where the resolution is only limited by the scale of the underlying building block. In that regard, block copolymers are particularly interesting, as they are known to spontaneously microphase separate into a variety of self-assembled nanostructures in the range of 10-100 nm [1]. Bulk morphologies have thus become increasingly relevant, e.g., for the bottom-up construction of nanoporous membranes [2–4], as templates for energy conversion [5–8], photonics [9], and as lithographic masks [10]. Aside from synthetically controlled parameters such as block weight fractions and block chemistries, supramolecular complexation of small-molecule additives selectively to one block is a versatile concept to generate functional morphologies, unusual geometries, and even introduce structural hierarchies [11–13]. Much effort has been invested to identify the impact of small-molecule complexation on the bulk behavior of diblock copolymers, where polystyrene-*block*-poly(4-vinylpyridine) (PS-*b*-P4VP) has been the most prominent example. Supramolecular binding motifs comprise phenols (pentadecyl phenol, hydroxy-styrene, azobenzenes) [14–21], carboxyls (cholesteryl-hemisuccinate and pyrene butyric acid) [22–24], alkylated sulfonic acids [25], and phenol/sulfonate mixtures [26,27]. The supramolecular additive is often introduced into the minority phase to change or fine-tune its geometry (e.g. from sphere to cylinder) and the lattice parameter as well as to allow hierarchical self-assembly involving the block copolymer length scale and the additive length scale. Besides hierarchical structuring or morphological transformations, hydrogen bonding additives were also used to selectively position nanoparticles [19] or to enrich the minority phase of bulk morphologies with inorganic precursors (templating) that upon successive oxidation formed well-ordered nanoparticle lattices (e.g. oxidation of ferrocene carboxylic acid to iron oxide) [28]. On the contrary, removal of additives from the minority phase leaves behind a porous scaffold as studied on fibers and membranes [15,29].

For more sophisticated arrangement of the nanophases, ABC triblock terpolymers and multiblock copolymers with three or more covalently linked polymer blocks become increasingly interesting [30–34]. The larger number of interaction parameters causes microphase separation into a rich variety of morphologies [35–37], quasi-crystalline patterns [38], knitting patterns [39], and even phases akin to metals [40]. Lamellar morphologies are of particular

interest, because cross-linkable middle domains that are “sandwiched” between terminal lamellae are the main source for a variety of polymeric Janus nanoparticles with specific geometry [41]. For instance, the lamella-sphere (*ls*), lamella-cylinder (*lc*) and lamella-lamella (*ll*) morphology of polystyrene-*block*-polybutadiene-*block*-poly(methyl methacrylate) (or poly(*tert*-butyl methacrylate)) triblock terpolymers (SBM or SBT) have been cross-linked to generate Janus spheres, cylinders and discs [42–44]. These geometries develop as a function of polybutadiene (PB) weight fraction, f_B, while keeping equally sized PS and PMMA blocks. In case of SBM, spherical PB domains are typically observed for $f_B \approx 0.05$-0.10, PB cylinders for $f_B \approx 0.10$-0.20, and lamellae for $f_B \approx 0.20$-0.50 (even larger PB domain forms the matrix for cylindrical or spherical phases of A and C). However, the delicate balance of interfacial energies between three polymer phases, χ_{AB}, χ_{AC}, and χ_{BC}, does not always allow the formation of the desired geometry even if proper weight fractions are synthesized. For instance, SBT terpolymers form a lamella-lamella bulk morphology almost independent of f_B, i.e., even at $f_B \approx 0.05$ where spheres are expected [44]. In addition to inaccessible geometries for some combinations of block chemistries, variation of the geometry of the middle phase is synthetically rather challenging, because each composition requires new synthesis.

Thus, a concept for modular tuning of the middle phase would be desirable to generate Janus nanoparticles with different geometry from the same triblock terpolymer. Blending homopolymer (or block copolymers) into the target phase is one approach to alter the bulk behavior [45] allowing the creation of intricate morphologies such as the knitting pattern [46] and non-centrosymmetric lamellae [47]. A supramolecular complexation of small-molecular additives, however, could allow a more accurate, continuous adjustment of the shape of the middle phase in very small steps to possibly identify other geometries besides sphere, cylinder and lamellae, towards a larger family of Janus nanostructures. Since mainly terminal block of ABC triblock terpolymers have been supramolecularly grafted [48–50], the effect of complexation on the sandwiched phase with two unlike phase boundaries is less known.

Here, we employed polystyrene-*block*-poly(4-vinylpyridine)-*block*-poly(*tert*-butyl methacrylate) (PS-*b*-P4VP-*b*-PT or S4VT) triblock terpolymers with varying P4VP weight fraction, $f_V = 0.17$, 0.12 and 0.05, and supramolecularly grafted the 4VP units with 4-(4-pentylphenylazo)phenol (5PAP) in nominal molar ratios of (5PAP/4VP) of $x = 0$, 0.25, 0.50, 0.75, and 1.0 (Scheme 1a). Due to the azobenzene group and short alkyl tail, the shape of 5PAP is relatively rod-like. After complexation in chloroform, we cast bulk films and analyzed the resulting morphologies with SAXS and TEM. Through gas-phase quaternization of P4VP with

methyl iodide to poly(*N*-methyl-4-pyridinium iodide) (P(Me4VP)I), we obtained the corresponding Janus nanostructures after re-dispersion of the bulk film in THF as good solvent for PS/PT (and non-solvent for the charged P(Me4VP)I phase) (Scheme 1b).

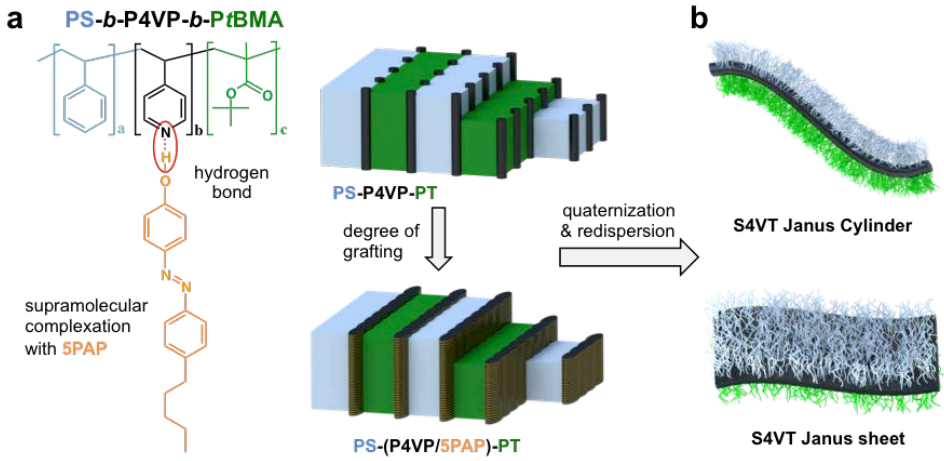

Scheme 1: Supramolecular grafting concept. a) Chemical structure of the employed S4VT triblock terpolymer and the 4-(4-pentylphenylazo)phenol (5PAP), and the transition from lamella-cylinder (*lc*) to lamella-lamella (*ll*) morphology. b) Quaternization with methyl iodide and re-dispersion in THF liberates Janus nanostructures with geometries corresponding the P4VP bulk phase.

Results and Discussion

For this work, we utilized S4VT triblock terpolymers with lamellae-forming endblocks PS and PT, but varied the weight fraction of the middle block, f_V. The synthesis of the three terpolymers, S4VT1-3, is described in detail in the Supporting Information and the terpolymer characteristics are summarized in Table 1.

Table 1: Polymer characteristics

Sample	DP_S[a]	DP_{4VP}[b]	DP_T[b]	f_S[c]	f_V	f_T	M_n[d]	PDI[d]
S4VT1	769	316	576	0.41	0.17	0.42	195	1.09
S4VT2	210	67	212	0.37	0.12	0.51	59	1.05
S4VT3	725	75	519	0.48	0.05	0.47	158	1.07

[a] Degree of polymerization determined with THF GPC and PS calibration; [b] Degree of polymerization determined with a combination of GPC and ^{1}H-NMR using the PS block as reference; [c] Weight fraction of PS calculated as $f_S=(DP_S*M_S)/M_n$; [d] Overall molecular weight of the terpolymers in [kg/mol] determined with GPC using THF + 0.25% TBABr as eluent and PS calibration for the first block.

Bulk films of all S4VT terpolymers were cast from chloroform and result in lamella-cylinder morphologies with P4VP cylinders irrespective of the P4VP weight fraction, here f_V= 0.05-0.17 (see Supporting Information for overview TEM images). S4VT is thus an example where synthetic variation of the middle block does not give rise to the expected morphologies, e.g. spheres at f_V= 0.05. The block volume and segment-segment interactions control the bulk behavior of polymer chains and are intrinsic parameters linked to the monomer chemistry and size. Supramolecular grafting with rod-like side groups can alter the block volume simply through the molar volume contribution of the additive, but also through increased segment rigidity, which affects chain packing, interfacial curvature and ultimately, the morphology (function of grafting density, which is also valid for flexible side groups) [51]. Here, we hydrogen bond 5PAP molecules in predefined molar ratios to the 4VP units of the middle block to create coil-comb-coil PS-*b*-(P4VP/5PAP)-*b*-PT triblock terpolymers during film casting and study the effect of increasing block straightening on the bulk behavior. In practice, we generate the coil-comb-coil configuration by adding specific molar amounts of 5PAP to the triblock terpolymer in chloroform and cast bulk films by slow solvent evaporation (for experimental details see Supporting Information). The hydrogen-bond acceptor (4VP) exhibits high coupling constants with the hydrogen-bond donor (phenolic hydroxyl of 5PAP), resulting in the comb-shaped middle block. The degree of straightening then depends on the grafting density of rod-like 5PAP molecules/moieties. During solvent evaporation the polymer chains start packing and microphase separate with the added 5PAP molecules mostly located in the P4VP phase. Figure S1 compares Fourier transform infrared (FTIR) spectra and photographic series of solvent-cast bulk films loaded with increasing molar fraction of 5PAP using nominal degrees of complexations from x = 0, 0.25, 0.50, 0.75, and 1.0, i.e., PS-*b*-(P4VP/5PAP)$_x$-*b*-PT, abbreviated as (S4VT1)$_x$. The S4VT1 samples show the complexation through hydrogen bonding. The IR peak of the free pyridine at 993 cm^{-1} decreases and shifts to 1008 cm^{-1} upon hydrogen bonding of 5PAP. Table 2 summarizes data obtained for the three terpolymers, S4VT1-3, supramolecularly complexed with azobenzene in 5 different molar ratios. While bulk films of the S4VT triblock terpolymers are colorless, the films with 5PAP become progressively more orange (color of the azobenzene). Yet, all bulk films remain transparent as sign for homogeneous distribution of the otherwise crystalline 5PAP.

Table 2: Mixing ratios of S4VT1-3/5PAP, observed bulk morphologies using TEM and SAXS as well as diffraction peaks and lattice vector lengths from SAXS

Sample code	5PAP [mol][a]	$f_{(4VP/5PAP)}$ [wt%] [b]	TEM	SAXS lattice type	Relative peaks	Lattice vector lengths [nm] [d]
$(S4VT1)_0$	0	0.17	*lc* [c]	*cyl*	1,√3,√4	*a* = 57 nm
$(S4VT1)_{0.25}$	0.25	0.25	*ll* [c]	*lc*	1,√2,√3,√9,√12	*a* = 62.9 nm *c* = 88.9 nm
$(S4VT1)_{0.50}$	0.50	0.32	*ll*	*lc*	1,√3,√4,√9,√12,√16	*a* = 55.4 nm *c* = 96 nm
$(S4VT1)_{0.75}$	0.75	0.37	*ll*	*lc*	1, 1.82, 2, 3, 3.64, 4	*a* = 52.2 nm *c* = 95 nm
$(S4VT1)_{1.0}$	1.0	0.42	*ll*	*lc*	1, 1.86, 2, 3.73, 4, 5	*a* = 51 nm *c* = 95 nm
$(S4VT2)_0$	0	0.12	*lc*	*lc*	1, 2, 2.24, 2.83, 3, 3.6, 4, 4.47, 5, 5.39, 6, 7	*a* = 23.1 nm *c* = 46.2 nm
$(S4VT2)_{0.25}$	0.25	0.18	*lpl* [c]	*ll*	1, 2, 3, 4, 5, 6, 7	*c* = 48.1 nm
$(S4VT2)_{0.50}$	0.50	0.24	*lpl*	*ll*	1, 2, 3, 4, 5, 6, 7, 8, 9	*c* = 47.5 nm
$(S4VT2)_{0.75}$	0.75	0.28	*ll*	*ll*	1, 2, 3, 4, 5, 6, 7	*c* = 44.8 nm
$(S4VT2)_{1.0}$	1.0	0.33	*ll*	*ll*	2, 3, 4, 5	*c* = 42.4 nm
$(S4VT3)_0$	0	0.05	*lc*	*lc*	1, 1.48, 2, 2.95, 3, 4	*a* = 30.8 nm *c* = 45.45 nm
$(S4VT3)_{0.25}$	0.25	0.08	*lc*	*lc*	1, 1.5, 2, 3, 3.17	*a* = 28.5 nm *c* = 42.9 nm
$(S4VT3)_{0.50}$	0.50	0.11	*lc*	*lc*	1, 1.46, 2, 2.92, 3, 3.08	*a* = 29.2 nm *c* = 42.6 nm
$(S4VT3)_{0.75}$	0.75	0.13	*lpl*	*lpl*	1, 1.44, 2, 2.88, 3, 3.05	*a* = 30.7 nm *c* = 44.3 nm
$(S4VT3)_{1.0}$	1.0	0.16	*lpl*	*lpl*	1, 1.41, 2, 2.83, 3	*a* = 32.0 nm *c* = 45.2 nm

[a] Loading of 5PAP in mol% compared to 4VP units; [b] weight fraction of P(4VP/5PAP) in dependence of the 5PAP loading; [c] bulk morphologies identified from TEM measurements: cylinder (*cyl*), lamella-cylinder (*lc*), lamella-lamella (*ll*) and lamella-perforated lamella (*lpl*); [d] The length of lattice vector **c** correspond to the lamellar long period L_0. Lattice vectors, **a** and **c**, are in perpendicular directions. See Scheme S1 in Supporting Information.

We first examine the microstructure of the $(S4VT1)_x$ series. To visualize the microstructure with transmission electron microscopy (TEM), bulk films were annealed at 110°C in vacuum, cut into thin films of about 100 nm thickness using an ultra-microtome, and deposited on carbon-coated copper grids. Figure 1 shows TEM images of bulk morphologies obtained for

$(S4VT1)_x$ with 5PAP loading of x = 0, 0.25, and 1.0, after staining the P4VP phase with iodine vapor for 2h (see Supporting Information). Pure S4VT1 features lamellae of both endblocks, PS (grey) and PT (bright), while P4VP can be clearly discerned as black dots at the interface of the PS/PT lamellae (Figure 1a). Note that PT degrades under electron-beam irradiation and thus appears thinner as in the native state. After evaluation of the structural features from different locations of several thin films, we attribute the dark phase to P4VP cylinders [52], which could be expected from a P4VP weight fraction of f_V = 0.17. The rather large overall molecular weight of S4VT1 (M_n = 195 kg/mol) results in large phase volumes. TEM image analysis yields a long period of L_0 = 105 nm, cylinder center-to-center distance of 54 nm and a cylinder diameter of D_{cyl} = 28 nm. We then studied the morphological evolution of this terpolymer with increasing molar fraction of 5PAP. With increasing 5PAP content, the lamellar features of PS/PT persist, yet the P4VP cylinders noticeably flatten at the lamellae interfaces as exemplified by $(S4VT1)_{0.25}$ corresponding to 25% grafting density along the P4VP chain (Figure 1b). Occasionally, the strongly elongated dark areas already merge into a continuous P4VP lamellae. This morphological evolution becomes more dominant at 50% and a complete transition to P4VP lamella occurs at 75% grafting density. Not surprisingly, the P(4VP/5PAP) lamella also appears at full grafting (Figure 1c). Overview images of all samples are given in the Supporting Information (Figure S2).

Measured distances in TEM have to be interpreted with care, as shearing during cutting, cutting angle towards the phases, and beam damage may have dramatic influence on domain sizes. Small-angle X-ray scattering (SAXS), on the other hand, is a non-invasive technique that gives more reliable average values of much larger sample volumes. For pure S4VT1, hexagonally packed long cylinder lattice was fitted to the SAXS data with lattice vector length a = 57 nm (Figure 1d, black curve). Broad diffraction peaks are produced by small average domain size of the hexagonal lattice. For pure S4VT1, diffraction peaks related to lamellar structure are not visible due to the small average domain size and low electron-density difference between the PS (0.566 mol/cm^3) and PT (0.561 mol/cm^3) phases. The SAXS data further supports the trend of a gradual shift from (*lc*)- to (*ll*)-morphology. For $(S4VT1)_{0.25}$, a lamellar period of c = 89 nm was calculated based on SAXS, which is in rather good agreement with the lamellar long period value found in TEM (80 – 95 nm). The cylinder center-to-center distance within the lamellar layer is a = 63 nm, which is slightly larger than 50 - 55 nm from TEM measurements. The SAXS curves of $(S4VT1)_x$ with x = 0.50, 0.75, and 1 show tetragonal structures with lamellar long periods of $c \approx 95$ nm and perpendicular lattice spacing of a = 55.4, a = 52.2

and a = 51 nm, respectively (see Table 1). The direction of the lattice vector, **c**, is from one lamellar layer to the next. In this direction the 5PAP loading has almost no effect. The perpendicular lattice vector, **a**, points from one cylinder to the next at the lamellar interface. The 5PAP loading decreases the cylinder-to-cylinder spacing in the direction of lattice vector **a**. This could be related to denser packing inside the P4VP phase, narrowing the cylinder spacing in the **a**-vector direction and directing the random-coil PS and PT phases to the lamellar layers. Although the peaks in SAXS are very broad it can be seen that with increasing 5PAP content the lamellar peaks become more pronounced whilst the peaks for the cylindrical phase vanish gradually and suggest a transition from cylinders to a lamellar phase. The SAXS curves of all $(S4VT1)_x$ samples are given in Supporting Figure S3.

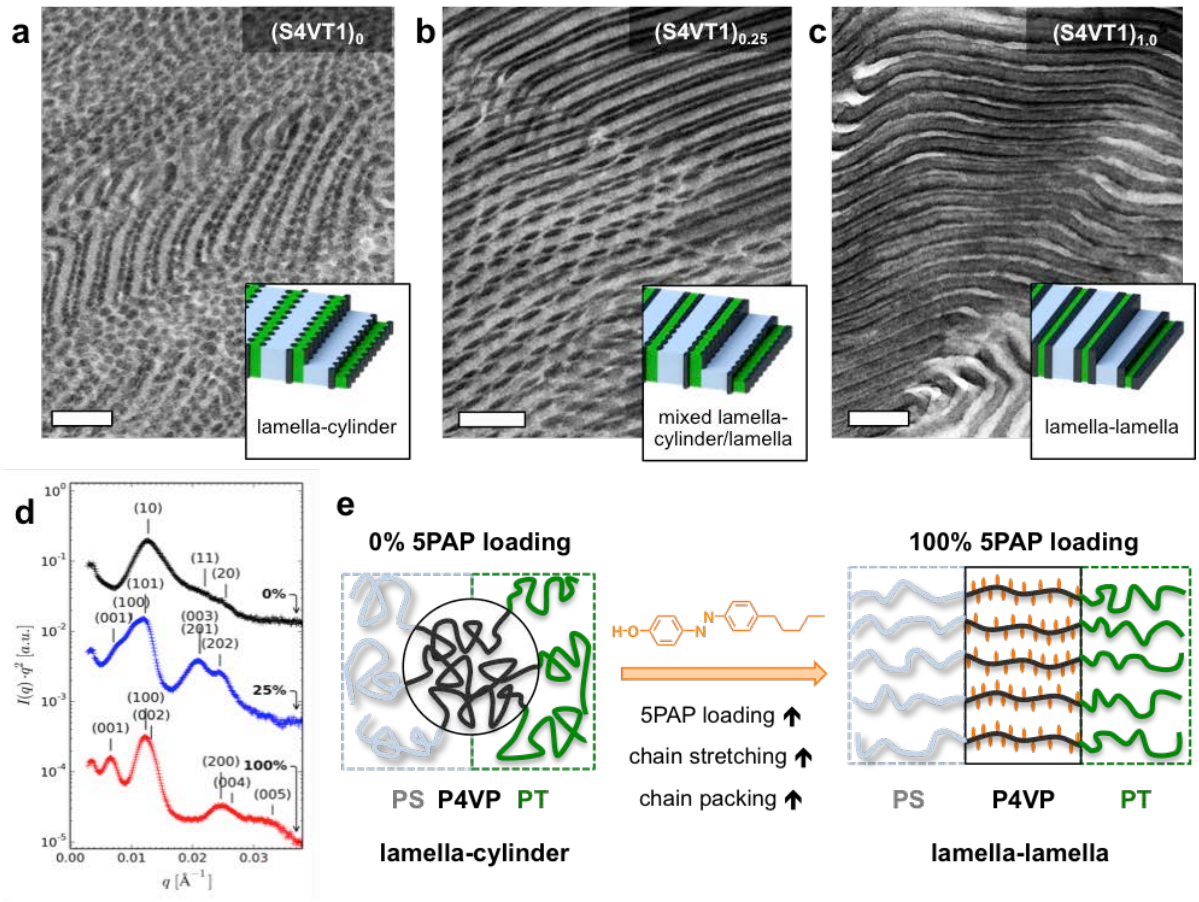

Figure 1. Morphological evolution of S4VT1 with increasing 5PAP loading. a-c) TEM images of $(S4VT1)_x$ with (a) x = 0, (b) x = 0.25, and (c) x = 1.0. Scale bars are 200 nm. d) SAXS data of the samples shown in (a-c). e) The suggested change of chain conformation after supramolecular grafting. Before grafting, the terpolymer chain adopts a coiled structure and the larger volumes of PS and PT

cause higher curvature at the PS/P4VP and P4VP/PT interface. After grafting, the rod-like 5PAP induces stretching of the P4VP chain, which leads to denser chain packing and flat (lamella) PS/P(4VP/5PAP) and P(4VP/5PAP)/PT interfaces.

There are several factors affecting the morphological transition from (*lc*)- to (*ll*)-morphology through supramolecular grafting of S4VT with the 5PAP. First, the additive increases the weight fraction, $f_{V/5PAP}$, of the middle phase from $f_{V/5PAP} = 0.17$ at 0% loading to $f_{V/5PAP} = 0.42$ at 100% loading. Hence, with increasing weight fraction a transition to a lamellar phase is expected by increase of phase volume alone. Additionally, another factors come into play. Complexation of small molecules is also known to alter chain packing and induce chain stretching with increasing grafting density [23,51]. The effect of chain stretching is sketched in Figure 1e for the two extreme cases of 0% and 100% loading. Prior to 5PAP grafting, S4VT chains adopt a thermodynamically favorable coiled conformation (Figure 1e, without 5PAP). The 5PAP corresponds to bulky side chains and induces chain straightening, which allows denser packing of the chains at the PS/P4VP and P4VP/PT interface. At full loading, the comb-like P(4VP/5PAP) chains pack more densely, promoting a planar interface that ultimately results in the (*ll*)-morphology (Figure 1e, full loading of 5PAP). As we will show later, dense chain packing is a convenient handle to manipulate morphology of the middle block even at low f_V. Besides chain packing also the interaction parameter χ between the blocks change. While $\chi_{SV} = 0.30$-0.35 [53] and $\chi_{VT} = 1.16$ are fairly high before complexation with 5PAP, the values decrease with increasing degree of loading to $\chi_{S\text{-}V5PAP} = 0.001$ and $\chi_{T\text{-}5PAP} = 0.015$ at full complexation (for calculations see Supporting Information). These values are even lower than for $\chi_{ST} = 0.025$ and promote spreading of the P4VP/5PAP block between the PS and PT end blocks and facilitates a transition from cylinder to lamellae.

Next, we examine S4VT2 with medium-sized middle block, $f_V = 0.12$, and a much lower overall molecular weight of $M_n = 59$ kg/mol (yet, still equal-sized endblocks). The annealing process at 110°C in vacuum for 24h has a strong effect on S4VT2 morphology. The lower overall molecular weight allows for large-scale alignment of the structure, further facilitated by plasticization of the P4VP block with added 5PAP where the T_g(P4VP) = 140 °C decreases to $T_g(P(4VP/5PAP)_{1.0}) \approx 50$ °C (similar to P4VP/2PAP and P4VP/8PAP) [54]. As a result, strikingly pronounced lamellar peaks develop in SAXS during annealing with reflexes visible up to the 9th order at 50% loading (Figure 2). At even higher degrees of complexation, diffraction peaks become less pronounced probably due to steric hindrances in the complexed P4VP

phase. SAXS of $(S4VT2)_0$ show tetragonal structure with a lamellar long period of c = 46.2 nm and perpendicular a = 23.1 nm period, which corresponds to the center-to-center distance of the P4VP cylinders at the lamella-cylinder interface. When the 5PAP loading reached 25% the morphology is clearly lamellar. SAXS measurements of $(S4VT2)_x$ show lamellar structures with decreasing long period c as a function of loading, from 48.1 nm at 25% to 42.4 nm at 100% (see Figure 3 and Table 1).

The first-order lamellar peak is weak mainly because of the small electron density difference between the thick PS (0.566 mol/cm^3) and PT (0.561 mol/cm^3) layers and almost symmetrical layer structure [49]. The relative SAXS peak heights from the S4VT2 samples with 25% to 100% 5PAP loading suggests two P4VP layers in a lamellar unit cell. In each unit cell PS and PT layers have almost equal thicknesses and a small electron-density difference with each other. The strong (002) reflection is mainly related to two P4VP layers in the unit cell having a high electron-density contrast with the PS and PT layers.

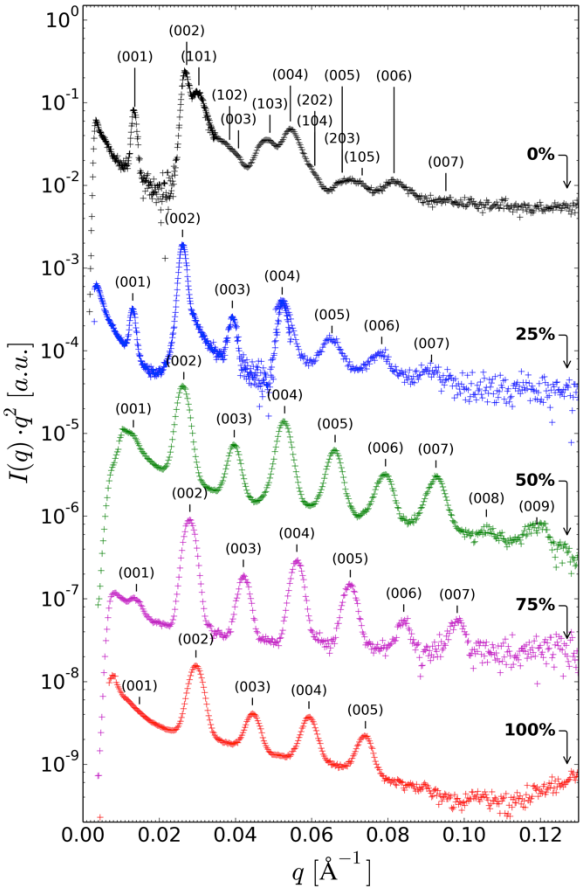

Figure 2. SAXS data for bulk films of $(S4VT2)_x$ with different amounts of 5PAP: 0% (black), 25% (blue), 50% (green), 75% (pink) and 100% (red).

From TEM analysis we likewise identify the (*lc*)-morphology for $(S4VT2)_0$. The long period L_0 = 48 nm as well as the cylinder diameter d_{cyl} = 10 nm is considerably smaller than for S4VT1, which is expected given the considerably smaller overall molecular weight (Figure 3a). SAXS measurements suggest a shift from (*lc*)- to (*ll*)-morphology induced by complexation with 25% 5PAP. On the contrary, the P(4VP/5PAP) phase clearly shows a perforated pattern in TEM flanked by PS and PT lamellae (Figure 3b). The patterned structure in $(S2VT2)_{0.25}$ may be a result of the volume increase of P4VP cylinders with 5PAP content. Cylinders start fusing together to form junction points leading to the perforated network (perforated lamella). Samples with 5PAP loadings $x > 0.50$ again form the (*ll*)-morphology visible as continuous dark stripes (Figure 3c). The sandwiched lamella is thermodynamically stable despite being unusually thin (d = 5 nm) [55]. Decreasing of the lamellar long period as a function of increasing 5PAP loading observed by SAXS could be related to morphological change from perforated lamellar structure (25% 5PAP loading) to lamella-lamella (100% 5PAP loading). Overview TEM images are shown in Supporting Figure S4.

The morphologies of $(S4VT2)_x$ are schematized in Figure 3d with P(4VP/5PAP) represented in black. Compared to the prominent sphere, cylinder and lamella phases, the perforated lamella is rarely observed. It has been reported for diblock copolymers [13], terpolymer core-shell systems [56–58] and block copolymer blends [59]. In ABC triblock terpolymer systems, the block arrangement commonly corresponds to a core-shell structure, where the middle block completely engulfs one of the end blocks leaving no interface between the A/C end blocks. In the present case, the perforated P(4VP/5PAP) layer is located at the interface of the PS and PT lamellae, hence, requiring PS and PT to form an additional interface within the perforation of P4VP. We have to speculate about the exact location of this interface, but the decreased repulsion between PS and P(4VP/5PAP) most likely allows the PS phase to fill out the “nanopores”. The (*ll*)-morphology for $(S4VT2)_{0.50\text{-}1.0}$ is a result of further volume increase and reduction of the interfacial repulsion between PS and P(4VP/5PAP). The reduced repulsion allows the middle phase to close the pores (larger PS/P(4VP/5PAP) interface) and the increased chain straightening promotes flattening of the middle phase into a lamella.

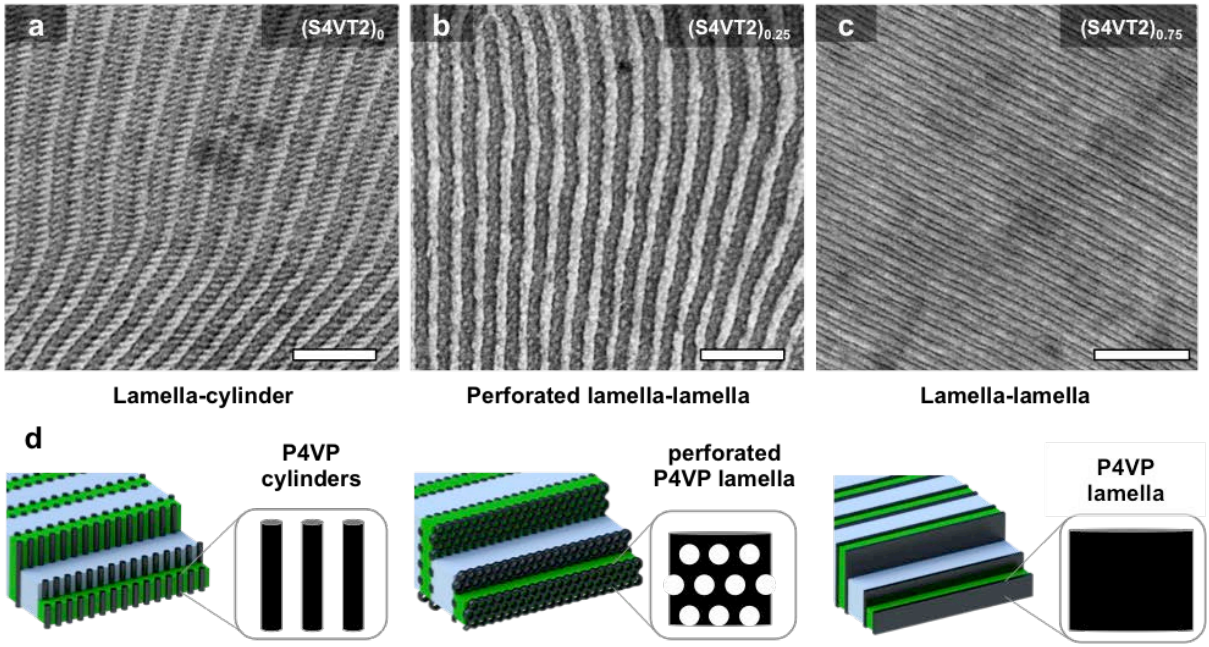

Figure 3. Morphological evolution of S4VT2 with increasing molar fraction of 5PAP. a-c) TEM images of $(S4VT2)_x$ with (a) $x = 0$, (b) $x = 0.25$, and (c) $x = 0.75$. Scale bars are 200 nm. d) Schematics of the (*lc*), (*lpl*) and (*ll*) phase. P4VP is in black, PS in light grey and PT in green.

From the three polymers studied, S4VT3 has the smallest P4VP block with $f_V = 0.05$. While the long period of $L_0 = 93$ nm in TEM is in good agreement with the $M_n = 158$ kg/mol, the P4VP domain forms cylinders with very small diameter $d_{cyl} = 5$ nm (Figure S6). Interestingly, the (*lc*)-morphology forms despite the low $f_V = 0.05$, where the (*ls*)-morphology is expected. Previous work on PS-*b*-PB-*b*-PT terpolymer showed that the PB phase spreads to form a lamella between the PS and PT phases even at $f_B = 0.05$ due to a very low χ_{BT} [44]. However, the formation of P4VP cylinders instead of spheres is unexpected for the S4VT system when comparing the χ-parameters. The interaction parameter of $\chi_{ST} = 0.025$ [60] is significantly lower than that of $\chi_{SV} = 0.30$-0.35 and $\chi_{VT} = 1.16$ (for calculations see Supporting Information). Although an empiric value of χ_{VT} is elusive, the calculated value (based on solubility parameters) suggests that P4VP and PT have the highest intrinsic incompatibility. Thus, PS/PT would be the most favorable interface supporting the formation of P4VP spheres. Yet, P4VP still forms cylinders as confirmed by TEM and SAXS measurements.

The SAXS curves of S4VT3 (Figure S7) suggests tetragonal packing of cylinders from 0% loading of 5PAP to 50% loading of 5PAP forming the (*lc*)-morphology. In azimuthal SAXS plot of $(S4VT3)_0$ (Figure S8) it can be observed that in tetragonal packing the lattice vectors **a** and **c** are clearly in perpendicular directions. In lattice spacing SAXS does not show any large

changes as a function of 5PAP loading. The aspect ratio of the unit cell *c/a* is 1.4 - 1.5, and it is almost constant throughout all S4VT3 samples until 50% loading of 5PAP. At 75% and 100% loadings, perforated lamellar structures are observed. (*lpl*)-morphology with ABAB packing has two lamellar layers in unit cell and the length of the lattice vector **c** equals the thickness of the two layers. The length of the lattice vector **a** equals the center-to-center distance of the holes in the perforated layers.

At full grafting, a very thin P(4VP/5PAP) lamella (d = 5 nm) with subtle structural differences is observed in TEM. As compared to the equilibrated (*lc*)-morphology, here the lamellae are more straightened out with domain sizes on the order of several dozen micrometers. The sandwiched P(4VP/5PAP) phase forms a perforated lamellar structure, comparable to that of $(S4VT2)_{0.25}$. Interestingly, S4VT1 with slightly higher f_V = 0.17 as compared to $(S4VT3)_{1.0}$ with $f_{V/5PAP}$ = 0.16 forms a (*lc*)-morphology while the latter forms a (*lpl*)-morphology (Figure 4 a, b). This hints towards the fact that the weight fraction of the middle block plays a subordinate role in the development of the morphology. A similar behavior has been described previously, where post-modification of the middle block of SBM triblock copolymers with (*ls*)-morphology with transition metal complexes showed morphological transitions to cylindrical and gyroidal structures. This was explained by the introduction of an asymmetric interfacial tension introduced by the post modification of the block copolymer rather than a significant change of the effective volume fraction of the middle block [61]. The perforated lamella in the present case is peculiar, because it is sandwiched between two other lamellae, which suggests a large interface between PS/P(4VP/5PAP) and PT/P(4VP/5PAP). The successive transition to P(4VP/5PAP) lamella can be interpreted as spreading. Spreading has been observed also for other ABC triblock terpolymer systems where $\chi_{AB} << \chi_{BC}$ [34]. Although here the initial χ-parameters do not favor such a behavior (χ_{SV} = 0.3-0.35; χ_{VT} = 1.16), the added 5PAP induces chain straightening of the P4VP phase and a change of the χ-parameters. The resulting dense chain packing of P(4VP/5PAP) promotes phase separation into a planar lamella even at low weight fractions but mostly a gradual change of the χ–parameter of P(4VP/5PAP) with PS and PT is expected. Based on solubility parameters, $\chi_{S\text{-}V5PAP}$ = 0.001 and $\chi_{T\text{-}5PAP}$ = 0.015 were estimated which drop even below that of χ_{ST} = 0.025 [60]. It has been shown for ABC triblock terpolymers with $\chi_{AB} \approx \chi_{BC} < \chi_{AC}$ spreading of the middle phase B between the two end block occur in order to exclude unfavorable A/C interface [34].

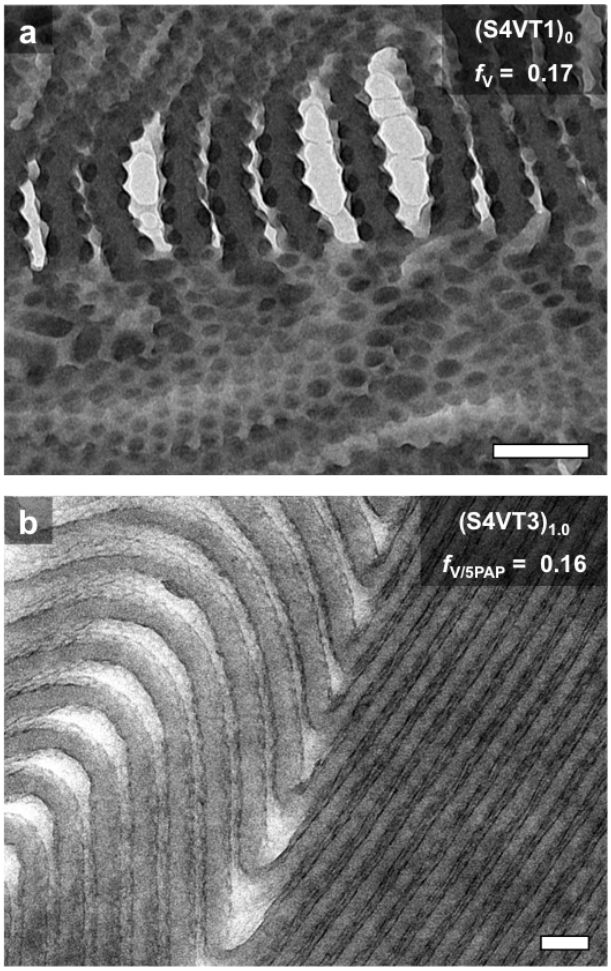

Figure 4. Two morphologies at comparable P4VP weight fraction but different 5PAP loading. a) S4VT1 with no 5PAP and $f_V = 0.17$ shows (*lc*)-morphology and b) S4VT3 with 100% 5PAP loading and $f_{V/5PAP} = 0.16$ shows a (*lpl*)-morphology due to the difference in chain packing. Scale bars are 100 nm.

An interesting feature of manipulating the middle block is that depending on the molar fraction of 5PAP, various morphologies of the P4VP phase can be modularly targeted by design. Hence, to demonstrate the formation of various types of Janus geometries with one single triblock terpolymer, we quaternized samples of S4VT2 with varying 5PAP content through gas-phase reaction of methyl iodide with the residual, non-hydrogen-bonded moieties of the P4VP middle phase to P(Me4VP)I and re-dispersed the modified bulk films in THF (see Supporting Information for experimental details and Figure S9). THF is a good solvent for PS and PT, while the P(Me4VP)I block remains insoluble. The supramolecular forces kinetically freeze the core of the respective Janus nanostructures and provide mechanical stability (Figure 5). In case of $(S4VT2)_0$, the (*lc*)-bulk morphology dispersed into individual Janus cylinders with a quaternized, charged P(Me4VP)I core decorated with PS and PT brushes as the phase-

separated hemispheres as schematically drawn in Figure 5a. A permanent fixation for potential applications is desirable and may be achieved using biiodides for covalent cross-linking or gelation with metal salts.

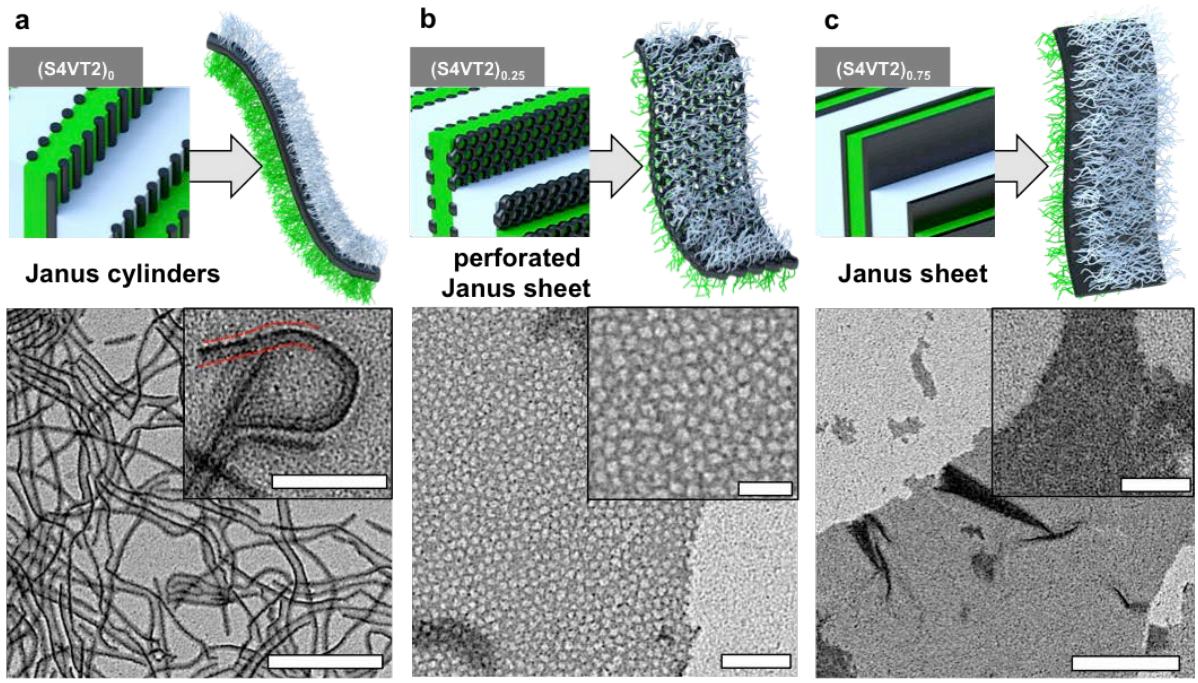

Figure 5. Schematic illustration and TEM images of the Janus particle formation *via* redispersion of bulk films of various morphologies to achieve Janus cylinders of $(S4VT2)_0$, perforated Janus lamellae of $(S4VT2)_{0.25}$ and a continuous Janus lamellae of $(S4VT2)_{0.75}$. Scale bars are 200 nm in the overview images and 100 nm in the insets, respectively.

The TEM image in Figure 5a and supporting overview images (Figure S10) depict cylindrical micelles up to several micrometers in length. The length thereby correlates with the domain size of the bulk film and is a measure for the quality of alignment. Longer annealing times improve the alignment and increase the domain size, which directly translates into cylinder length. The close-up illustrates the Janus character of an individual Janus cylinder where all three phases can be distinguished. The P4VP backbone is the black stripe (iodine staining), the dark grey hemisphere represents the PS phase while PT appears bright due to *e*-beam degradation. The reason why not all cylinders display this Janus structure in TEM is attributed to the fact that PS has a slight preference towards the carbon film of the TEM grid resulting in Janus cylinders facing with PS side towards the grid [62]. The TEM image in Figure 5b and the sketch both show a nanoporous Janus sheet as formed by $(S4VT2)_{0.25}$ after quaternization and re-dispersion in THF (see also supporting overview image Figure S11). The mesh of

P(Me4VP)I appears dark, while neither PS nor PT are visible. This is because the high-aspect-ratio sheets always lie flat on the carbon film with PS/PT located on top or on bottom of the sheet. A more detailed analysis of this novel nanostructure is done below. For high 5PAP loadings as, e.g. in $(S4VT2)_{0.75}$, a continuous lamella forms in the bulk and consequently we find a continuous Janus sheet in solution (Figure 5c and S12). The chemistry of these Janus nanostructurs offers versatility for future studies, as the PT phase can be hydrolyzed and P4VP cross-linked with various functional reagents.

The perforated Janus sheet is a most peculiar and interesting structure. From the AFM height image (Figure 6a), we find a sheet of continuous height with darker circular areas corresponding to holes within the P(4VP/5PAP) layer. The average height of the sheet is about h = 13 nm (Figure 6b, blue line), and ca. 26 nm for a double layer of overlapping sheets (Figure 6b, red line). These values are significantly lower than half the long period of $L_0/2 \approx 24$ nm (corresponds to one SVT sequence) and may be explained by the collapse of the PS/PT chains upon solvent evaporation during sample preparation. In the bulk state, each PS (or PT) lamella consists of interpenetrating chains contributed from two P4VP lamellae. Thus, the volume of the PS (or PT) phase per individual sheet is reduced to half compare to that in bulk when redispersed and dried. The soluble blocks collapse into a smaller volume on top of the sheet upon evaporation of the solvent which is why the measured h = 13 nm is smaller than $L_0/2 \approx 24$ nm of the bulk phase. Most importantly, the sheets exhibit a continuous height with only minor variations and over a distance of several micrometers proving the 2D character. Fourier transform of the TEM image in Figure 6c shows a slightly elliptical shape corresponding to a variation of inter-pore distances, i.e., about 30 nm in vertical and 27 nm in horizontal direction. This slight distortion may occur because of irregular arrangement of the non-spherical pores or originate from an artifact during sample preparation, i.e. either the sheet does not lie flat on the carbon film or solvent evaporation induced some distortion. The perforated Janus sheets are interesting to study as they represent a “nanoporous membrane” with a pore diameter of about 20 nm and two different chemical structures of both sides of the membrane (selective permeation). Adjusting the molecular weight of the ABC triblock terpolymer would give rise to a variety of pore diameters, while the pH-responsive mesh (e.g. at low quaternization) could result in reversible opening/closing of the pores for nanofiltration applications.

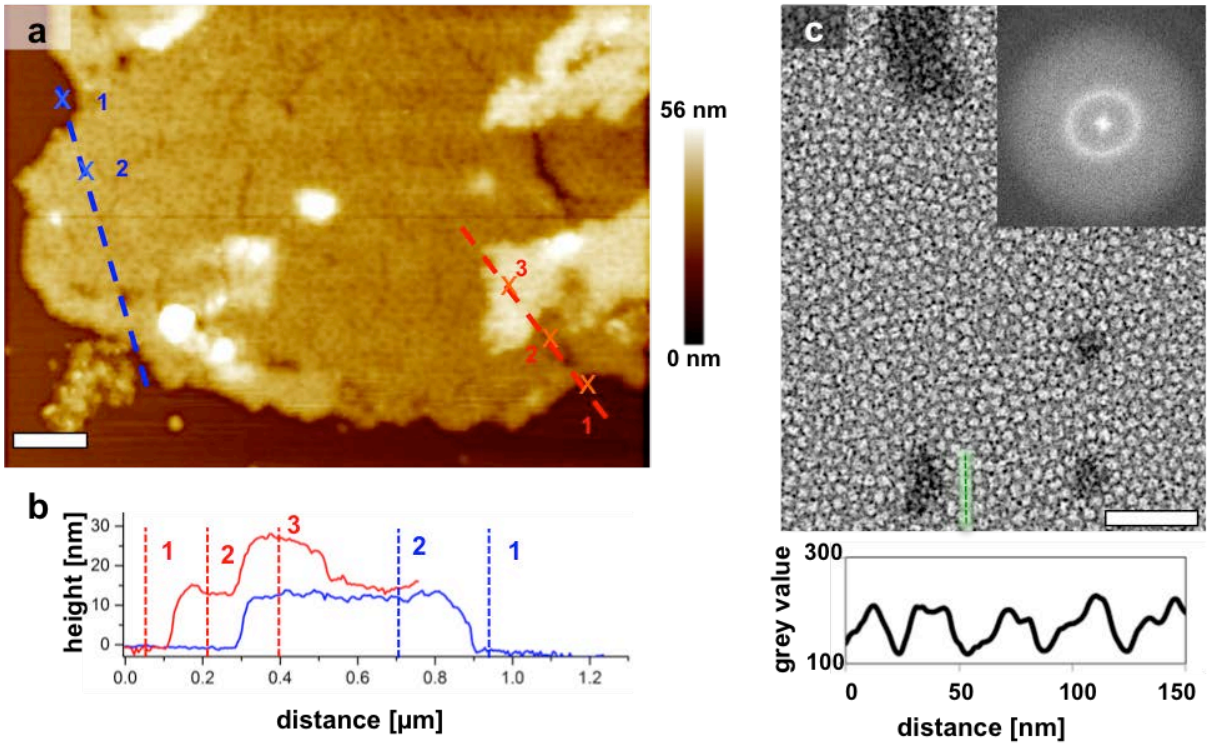

Figure 6. Analysis of perforated Janus sheet of $(S4VT2)_{0.25}$. a) AFM height image of a perforated sheet. b) Height plots as marked in (a) of a single layer sheet with h = 13nm (blue line) and a double layer with h = 26nm (red line). c) TEM image of the nanoporous sheet, corresponding FFT and grey scale analysis of the green marked region. Scale bars are 200 nm.

Conclusion

In summary, we have shown that hydrogen bonding is a versatile tool to tune the shape of individual phases of ABC triblock terpolymer morphologies. This was demonstrated on loading of S4VT triblock terpolymer morphologies with 4-(4-pentylphenylazo)phenol, 5PAP, where the 4VP repeating units act as hydrogen-bond acceptor and the phenol of 5PAP as hydrogen-bond donor. Although S4VT forms (*lc*)-morphologies irrespective of the weight fraction of the 4VP block, hydrogen bonding in proper molar fractions changed the morphology to (*ll*) in all cases. The rod-like molecule noticeably deforms the P4VP microphase as compromise of phase separation at two length scales: i) at a molecular level by chain packing inside the P(4VP/5PAP) phase and ii) at the nanoscale through enthalpic repulsion of the three polymer phases. We further identified interesting geometries at low and medium loading of 5PAP such as flattened cylinders and perforated lamellae. These bulk morphologies formed the basis for the synthesis of Janus particles with various geometries such as Janus cylinders, perforated

Janus membranes and Janus sheets. Janus particles are of general interest for various applications, where a high interfacial activity is desirable such as compatibilizers for immiscible polymer blends, emulsifiers, and compatibilizers for carbon nanotubes [63–65]. Tuning the geometry of the Janus particles by modifying a single ABC triblock terpolymer is a facile strategy and allows direct comparison of the shape-dependent performance without the need of changing the chemistry or composition. The concept further allows generating target geometries that may be inaccessible for particular combinations of block chemistries.

References

[1] F.H. Schacher, P.A. Rupar, I. Manners, Functional block copolymers: nanostructured materials with emerging applications., Angew. Chem. Int. Ed. 51 (2012) 2–25.

[2] R.M. Dorin, W.A. Phillip, H. Sai, J. Werner, M. Elimelech, U. Wiesner, Designing block copolymer architectures for targeted membrane performance, Polymer. 55 (2014) 347–353.

[3] V. Abetz, Isoporous block copolymer membranes, Macromol. Rapid Commun. 36 (2015) 10–22.

[4] M. Ulbricht, Advanced functional polymer membranes, Polymer. 47 (2006) 2217–2262.

[5] M.C. Orilall, U. Wiesner, Block copolymer based composition and morphology control in nanostructured hybrid materials for energy conversion and storage: solar cells, batteries, and fuel cells., Chem. Soc. Rev. 40 (2011) 520–535.

[6] T. Lunkenbein, M. Kamperman, Z. Li, C. Bojer, M. Drechsler, S. Förster, U. Wiesner, A.H.E. Müller, J. Breu, Direct synthesis of inverse hexagonally ordered diblock copolymer/polyoxometalate nanocomposite films., J. Am. Chem. Soc. 134 (2012) 12685–92.

[7] B. Smarsly, M. Antonietti, Block copolymers as templates for the generation of mesostructured inorganic materials, in: M. Lazzari, G. Liu, S. Lecommandoux (Eds.), Block Copolym. Nanosci., WILEY-VCH Verlag, Weinheim, 2006: pp. 291–307.

[8] E.J.W. Crossland, M. Kamperman, M. Nedelcu, C. Ducati, U. Wiesner, D.-M. Smilgies, G.E.S. Toombes, M.A. Hillmyer, S. Ludwigs, U. Steiner, H.J. Snaith, A bicontinuous double gyroid hybrid solar cell, Nano Lett. 9 (2009) 2807–2812.

[9] M. Stefik, S. Guldin, S. Vignolini, U. Wiesner, U. Steiner, Block copolymer self-assembly for nanophotonics, Chem. Soc. Rev. 44 (2015) 5076–5091.

[10] C. Tang, E.M. Lennon, G.H. Fredrickson, E.J. Kramer, C.J. Hawker, Evolution of block

copolymer lithography to highly ordered square arrays., Science. 322 (2008) 429–432.

[11] O. Ikkala, G. ten Brinke, Functional materials based on self-assembly of polymeric supramolecules., Science. 295 (2002) 2407–2409.

[12] G. ten Brinke, K. Loos, I. Vukovic, G.G. du Sart, Hierarchical self-assembly of two-length-scale multiblock copolymers, J. Phys. Condens. Matter. 23 (2011) 284110.

[13] I. Vukovic, G. Ten Brinke, K. Loos, Hexagonally perforated layer morphology in PS-b-P4VP(PDP) supramolecules, Macromolecules. 45 (2012) 9409–9418.

[14] J. Ruokolainen, G. Ten Brinke, O. Ikkala, Supramolecular polymeric materials with hierarchical structure-within-structure morphologies, Adv. Mater. 11 (1999) 777–780.

[15] A. Sidorenko, I. Tokarev, S. Minko, M. Stamm, Ordered reactive nanomembranes/nanotemplates from thin films of block copolymer supramolecular assembly, J. Am. Chem. Soc. 125 (2003) 12211–12216.

[16] T. Ruotsalainen, J. Turku, P. Hiekkataipale, U. Vainio, R. Serimaa, G. Ten Brinke, A. Harlin, J. Ruokolainen, O. Ikkala, Tailoring of the hierarchical structure within electrospun fibers due to supramolecular comb-coil block copolymers: polystyrene-block-poly(4-vinyl pyridine) plasticized by hydrogen bonded pentadecylphenol, Soft Matter. 3 (2007) 978–985.

[17] J. De Wit, G.A. Van Ekenstein, E. Polushkin, K. Kvashnina, W. Bras, O. Ikkala, G. Brinke, Self-assembled poly(4-vinylpyridine)-surfactant systems using alkyl and alkoxy phenylazophenols, Macromolecules. 41 (2008) 4200–4204.

[18] W. Van Zoelen, E. Polushkin, G. Brinke, Hierarchical terrace formation in PS-b-P4VP(PDP) supramolecular thin films, Macromolecules. 41 (2008) 8807–8814.

[19] Y. Zhao, K. Thorkelsson, A.J. Mastroianni, T. Schilling, J.M. Luther, B.J. Rancatore, K. Matsunaga, H. Jinnai, Y. Wu, D. Poulsen, J.M.J. Fréchet, a P. Alivisatos, T. Xu, Small-molecule-directed nanoparticle assembly towards stimuli-responsive nanocomposites., Nat. Mater. 8 (2009) 979–985.

[20] I. Vukovic, G. ten Brinke, K. Loos, Hexagonally Perforated Layer Morphology in PS-b-P4VP(PDP) Supramolecules, Macromolecules. 45 (2012) 9409–9418.

[21] R. Ahmed, A. Priimagi, C.F.J. Faul, I. Manners, Redox-active, organometallic surface-relief gratings from azobenzene-containing polyferrocenylsilane block copolymers, Adv. Mater. 24 (2012) 926–931.

[22] J.T. Korhonen, T. Verho, P. Rannou, O. Ikkala, Self-assembly and hierarchies in pyridine-containing homopolymers and block copolymers with hydrogen-bonded

cholesteric side-chains, Macromolecules. 43 (2010) 1507–1514.

[23] A.J. Soininen, I. Tanionou, N. ten Brummelhuis, H. Schlaad, N. Hadjichristidis, O. Ikkala, J. Raula, R. Mezzenga, J. Ruokolainen, Hierarchical Structures in Lamellar Hydrogen Bonded LC Side Chain Diblock Copolymers, Macromolecules. 45 (2012) 7091–7097.

[24] B.K. Kuila, E.B. Gowd, M. Stamm, Supramolecular assembly of poly(styrene)-b-poly(4-vinylpyridine) and 1-pyrenebutyric acid in thin film and their use for nanofabrication, Macromolecules. 43 (2010) 7713–7721.

[25] H. Kosonen, S. Valkama, J. Ruokolainen, M. Torkkeli, R. Serimaa, G. Ten Brinke, O. Ikkala, One-dimensional optical reflectors based on self-organization of polymeric comb-shaped supramolecules, Eur. Phys. J. E. 10 (2003) 69–75.

[26] J. Ruokolainen, R. Mäkinen, M. Torkkeli, T. Mäkelä, R. Serimaa, G. ten Brinke, O. Ikkala, Switching supramolecular polymeric materials with multiple length scales, Science. 280 (1998) 557–560.

[27] S. Valkama, H. Kosonen, J. Ruokolainen, T. Haatainen, M. Torkkeli, R. Serimaa, G. ten Brinke, O. Ikkala, Self-assembled polymeric solid films with temperature-induced large and reversible photonic-bandgap switching., Nat. Mater. 3 (2004) 872–876.

[28] B.K. Kuila, M.S. Rama, M. Stamm, Supramolecular assembly of poly(styrene)-b-poly(4-vinylpyridine) and ferroceneacetic acid: an easy way to large-scale controllable periodic arrays of iron oxide nanomaterials., Adv. Mater. 23 (2011) 1797–800.

[29] R. Mäki-Ontto, K. De Moel, W. De Odorico, J. Ruokolainen, M. Stamm, G. Ten Brinke, O. Ikkala, “Hairy tubes”: mesoporous materials containing hollow self-organized cylinders with polymer brushes at the walls, Adv. Mater. 13 (2001) 117–121.

[30] C. Auschra, R. Stadler, Synthesis of block copolymers with poly(methyl methacrylathe): P(B-b-MMA), P(EB-b-MMA), P(S-b-B-b-MMA) and P(S-b-EB-b-MMA), Polym. Bull. 30 (1993) 257–264.

[31] C. Auschra, R. Stadler, New ordered morphologies in ABC triblock copolymers, Macromolecules. 26 (1993) 2171–2174.

[32] S. Ludwigs, A. Böker, V. Abetz, A.H.E. Müller, G. Krausch, Phase behavior of linear polystyrene-block-poly(2-vinylpyridine)-block-poly(tert-butyl methacrylate) triblock terpolymers, Polymer. 44 (2003) 6815–6823. doi:10.1016/j.polymer.2003.07.001.

[33] F. Schacher, J. Yuan, H.G. Schoberth, A.H.E. Müller, Synthesis, characterization, and bulk crosslinking of polybutadiene-block-poly(2-vinyl pyridine)-block-poly(tert-butyl

methacrylate) block terpolymers, Polymer. 51 (2010) 2021–2032.

[34] T.I. Löbling, P. Hiekkataipale, A. Hanisch, F. Bennet, H. Schmalz, O. Ikkala, A.H. Gröschel, A.H.E. Müller, Bulk morphologies of polystyrene-block-polybutadiene-block-poly(tert-butyl methacrylate) triblock terpolymers, Polymer. 72 (2015) 479–489.

[35] F.S. Bates, G.H. Fredrickson, Block copolymers—designer soft materials, Phys. Today. 52 (1999) 32–38.

[36] V. Abetz, P.F.W. Simon, Phase behaviour and morphologies of block copolymers, in: Adv. Polym. Sci., 2005: pp. 125–212.

[37] R. Stadler, C. Auschra, J. Beckmann, U. Krappe, I. Voigt-Martin, L. Leibler, Morphology and thermodynamics of symmetric poly(A-block-B-block-C) triblock copolymers, Macromolecules. 28 (1995) 3080–3091.

[38] K. Hayashida, T. Dotera, A. Takano, Y. Matsushita, Polymeric quasicrystal: mesoscopic quasicrystalline tiling in ABC star polymers, Phys. Rev. Lett. 98 (2007) 195502.

[39] U. Breiner, U. Krppe, R. Stadler, Evolution of the " knitting pattern " morphology in ABC triblock copolymers, Macromol. Rapid Commun. 17 (1996) 567–575.

[40] S. Lee, M.J. Bluemle, F.S. Bates, Discovery of a Frank-Kasper sigma phase in sphere-forming block copolymer melts., Science. 330 (2010) 349–53.

[41] A. Walther, A.H.E. Müller, Janus particles: synthesis, self-assembly, physical properties, and applications., Chem. Rev. 113 (2013) 5194–5261.

[42] R. Erhardt, A. Böker, H. Zettl, H. Kaya, W. Pyckhout-Hintzen, G. Krausch, V. Abetz, A.H.E. Müller, Janus micelles, Macromolecules. 34 (2001) 1069–1075.

[43] Y. Liu, V. Abetz, A.H.E. Müller, Janus cylinders, Macromolecules. (2003) 7894–7898.

[44] A. Walther, X. André, M. Drechsler, V. Abetz, A.H.E. Müller, Janus discs., J. Am. Chem. Soc. 129 (2007) 6187–6198.

[45] V. Abetz, T. Goldacker, Formation of superlattices via blending of block copolymers, Macromol. Rapid Commun. 21 (2000) 16–34.

[46] T. Goldacker, V. Abetz, A new way to the "knitting pattern" via blending of ABC triblock copolymers, Macromol. Rapid Commun. 20 (1999) 415–418.

[47] T. Goldacker, V. Abetz, R. Stadler, I. Erukhimovich, L. Leibler, Non-centrosymmetric superlattices in block copolymer blends, Nature. 398 (1999) 137–139.

[48] S. Jiang, A. Göpfert, V. Abetz, Novel morphologies of block copolymer blends via hydrogen bonding, Macromolecules. 36 (2003) 6171–6177.

[49] G. Gobius du Sart, I. Vukovic, G. Alberda Van Ekenstein, E. Polushkin, K. Loos, G. ten

Brinke, Self-assembly of supramolecular triblock copolymer complexes, Macromolecules. 43 (2010) 2970–2980.

[50] G.G. du Sart, I. Vukovic, Z. Vukovic, E. Polushkin, P. Hiekkataipale, J. Ruokolainen, K. Loos, G. ten Brinke, Nanoporous network channels from self-assembled triblock copolymer supramolecules., Macromol. Rapid Commun. 32 (2011) 366–70.

[51] G.H. Fredrickson, Surfactant-induced lyotropic behavior of flexible polymer solutions, Macromolecules. 26 (1993) 2825–2831.

[52] R. Erhardt, Amphiphile oberflächenkompartimentierte Polymermicellen mit vernetztem Kern, University of Bayreuth, 2001.

[53] G. Gobius, R. Rachmawati, V. Voet, G.A. Van Ekenstein, E. Polushkin, G. Brinke, K. Loos, Poly(tert-butyl methacrylate-b-styrene-b-4-vinylpyridine) triblock copolymers : synthesis , interactions , and self-assembly, Macromolecules. 41 (2008) 6393–6399.

[54] M. Poutanen, O. Ikkala, A. Priimagi, Structurally Controlled Dynamics in Azobenzene-Based Supramolecular Self-Assemblies in Solid State, Macromolecules. (2016). doi:10.1021/acs.macromol.6b00562.

[55] W. Shi, A.L. Hamilton, K.T. Delaney, G.H. Fredrickson, E.J. Kramer, C. Ntaras, A. Avgeropoulos, N. a. Lynd, Creating extremely asymmetric lamellar structures via fluctuation-assisted unbinding of miktoarm star block copolymer alloys, J. Am. Chem. Soc. 137 (2015) 6160–6163.

[56] E. Betthausen, M. Dulle, C. Hanske, M. Müll, A. Fery, S. Förster, F.H. Schacher, A.H.E. Müller, Nanoporous sheets and cylinders via bulk templating of triblock terpolymer/homopolymer blends, Macromolecules. 47 (2014) 6289–6301.

[57] F.H. Schacher, H. Sugimori, S. Hong, H. Jinnai, A.H.E. Müller, Tetragonally Perforated Lamellae of Polybutadiene-block-poly(2-vinylpyridine)-block-poly(tert- butyl methacrylate) (BVT) Triblock Terpolymers in the Bulk: Preparation, Cross-Linking, and Dissolution, Macromolecules. 45 (2012) 7956−7963.

[58] S. Ludwigs, A. Böker, A. Voronov, N. Rehse, R. Magerle, G. Krausch, Self-assembly of functional nanostructures from ABC triblock copolymers., Nat. Mater. 2 (2003) 744–747.

[59] K. Markgraf, V. Abetz, Superlattices in block copolymer blends with attractive interactions, E-Polymers. 015 (2001) 1–17.

[60] D.W. Schubert, M. Stamm, A.H.E. Müller, Neutron reflectometry studies on the interfacial width between polystyrene and various poly(alkylmethacrylates), Polym.

Eng. Sci. 39 (1999) 1501–1507.

[61] L. Bronstein, M. Seregina, P. Valetsky, U. Breiner, V. Abetz, R. Stadler, Transition metal complex induced morphology change in an ABC triblock copolymer, Polym. Bull. 368 (1997) 361–368.

[62] A.H. Gröschel, A. Walther, T.I. Löbling, J. Schmelz, A. Hanisch, H. Schmalz, A.H.E. Müller, Facile, solution-based synthesis of soft, nanoscale janus particles with tunable janus balance, J. Am. Chem. Soc. 134 (2012) 13850–13860.

[63] R. Bahrami, T.I. Löbling, A.H. Gröschel, H. Schmalz, A.H.E. Müller, V. Altstädt, The impact of Janus nanoparticles on the compatibilization of immiscible polymer blends under technologically relevant conditions, ACS Nano. 8 (2014) 10048–10056.

[64] A. Walther, M. Hoffmann, A.H.E. Müller, Emulsion polymerization using Janus particles as stabilizers., Angew. Chemie Int. Ed. 47 (2008) 711–714.

[65] A.H. Gröschel, T.I. Löbling, P.D. Petrov, M. Müllner, C. Kuttner, F. Wieberger, A.H.E. Müller, Janus micelles as effective supracolloidal dispersants for carbon nanotubes., Angew. Chemie Int. Ed. 52 (2013) 3602–3606.

Acknowledgments

This work was carried out under the Academy of Finland's Centre of Excellence Programme (2014-2019) and supported by ERC-2011-AdG (291364-MIMEFUN). The authors further made use of the Aalto University Nanomicroscopy Center (Aalto-NMC) premises.

Competing financial interests

The authors declare no competing financial interests.

Additional information

Correspondence and requests for materials should be addressed to O.I. or A.H.G.